

# Experimental Evaluation of a Soft-Switching DC/DC Converter for Fuel Cell Vehicle Applications\*

Gui-Jia Su<sup>1</sup>, Fang Z. Peng<sup>1,2</sup> and Donald J. Adams<sup>1</sup>

<sup>1</sup>Oak Ridge National Laboratory, 2360 Cherahala Blvd., Knoxville, TN 37932, [sugi@ornl.gov](mailto:sugi@ornl.gov)

<sup>2</sup>Michigan State University, 2120 Engineering Building, East Lansing, MI 48824-1226, [fzpeng@egr.msu.edu](mailto:fzpeng@egr.msu.edu)

**Abstract** - A soft-switched, isolated bi-directional DC/DC converter has been developed for fuel cell powered electric vehicles (FCPEV), in which the 12 V battery for the vehicle accessory loads is also used to start up the fuel cells and to store the energy captured during regenerative braking. The DC/DC converter interfaces the low voltage battery to the fuel cell powered higher voltage DC bus system (255 V ~ 425 V). Dual half-bridges interconnected through a transformer are employed to minimize the number of switching devices and their associated gate drive components. The transformer provides voltage level matching and galvanic isolation for safety requirements. Snubber capacitors and the transformer leakage inductance are utilized to achieve zero-voltage-switching (ZVS). Therefore, no extra resonant components are required for ZVS, further reducing component count. The inherent soft-switching capability and the low component count of the converter allows efficient power conversion and compact packaging. A prototype was built and successfully tested. This paper presents design considerations and testing data to evaluate the prototype's performance against the requirements for FCPEV applications.

## I. INTRODUCTION

Fuel cells show great promise as the primary power source for next-generation propulsion, because they generate clean electricity directly and efficiently while leaving only nonpolluting byproducts—water and heat [1]. An auxiliary energy storage device is required for start-up and for storing the energy captured through regenerative braking in electric vehicle applications, because the present fuel cell technology lacks energy storage capability. One way to accomplish this is to utilize the vehicle 12 V battery with a bi-directional dc-dc converter to maintain compatibility with the majority of today's automobile loads, as shown in Fig.1. During vehicle

starting, the high-voltage bus is boosted up to around 280 V by the dc/dc converter drawing power from the 12 V battery. This high-voltage bus then supplies power for the fuel cell compressor motor expanding unit (CMEU) controller and brings up the fuel cell voltage, which in turn feeds back to the high-voltage bus to release the loading from the battery. In addition, the battery absorbs the energy captured by regenerative braking through the traction motor.

This application requires a dc/dc converter with a relatively high power rating of 1.6 kW continuous, aside from bi-directional power control capability. The converter also needs to provide galvanic isolation between the low- and high-voltage buses to meet safety requirements. Further, soft switching is preferred over hard switching because of the reduced level of electromagnetic interference (EMI) and switching losses. Other expected requirements for this converter are outlined as follows.

- The terminal voltage of the battery can swing from 8 V to 16 V during either direction of power flow.
- The nominal voltage of the high voltage bus is 288 V, with an operating range of from 255 V to 425V.
- A maximum battery charging power of 5 kW is required for a maximum duration of 20 s during regeneration. Each such charging event is at least 1 minute apart.
- The high-voltage bus capacitance  $C_o$  must be less than 2000  $\mu$ F.
- Start-up time is less than 200 ms with load engaged when the voltage of the high-voltage bus is higher than 255 V.

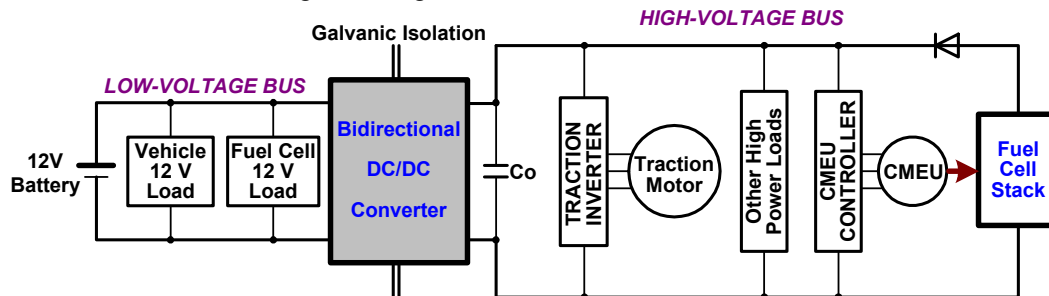


Fig. 1. A conceptual diagram of a fuel cell-powered propulsion system.

\* Prepared by Oak Ridge National Laboratory, managed by UT-Battelle, LLC, for the U.S. Dept. of Energy under contract DE-AC05-00OR22725. The submitted manuscript has been authored by a contractor of the U.S. Government under contract DE-AC05-00OR22725. Accordingly, the U.S. Government retains a nonexclusive, royalty-free license to publish or reproduce the published form of this contribution, or allow others to do so, for U.S. Government purposes.

Most of the existing dc/dc converter topologies are of low power or unidirectional power flow and cannot meet the requirements [2, 3]. Recently, high-power, bi-directional dc/dc converters with soft-switching operation and galvanic isolation have been introduced in the literature [4–7]. These converters are regarded as candidates for automotive applications because they have the advantages of reduced switching losses and EMI. However, they are unable to achieve high power density, high reliability, and low cost because the requirements for dedicated devices and/or complicated control schemes for soft switching result in bulky and costly implementation.

The dc/dc converter in [8], developed for FCPEV applications, employs a novel soft-switching circuit for a dual full-bridge topology. While this technique could significantly improve efficiency and power density over the existing high-power dc/dc converters, the large number of active switches and associated components and complexity of control are concerns in light of the low cost and high reliability demands for automotive applications. Aiming at reducing component count and achieving soft-switching simultaneously, a new dc/dc converter has been developed based on a half-bridge topology [9]. It utilizes snubber capacitors and the transformer leakage inductance to achieve zero-voltage-switching (ZVS). Therefore, no extra resonant components are required for ZVS, further reducing component count. The inherent soft-switching capability and the low component count of the converter allow high power density, efficient power conversion, and compact packaging. A 1.6 kW prototype was built and successfully tested. This paper presents design considerations and testing data to evaluate the prototype’s performance against the requirements for FCPEV applications.

## II. DC/DC CONVERTER DESCRIPTION

### A. Circuit Description

Fig. 2 shows the bi-directional dc/dc converter, which mainly consists of an unsymmetrical half-bridge converter on the low-voltage side (LVS), a symmetrical half-bridge converter on the high-voltage side (HVS), and a high-frequency transformer,  $T_r$  that links the two converters. The transformer provides the required galvanic isolation to meet safety requirements and voltage level matching. The leakage inductance of the transformer is utilized as the intermediate energy storing and transferring element. Control of the power flow between the low- and high-voltage sides can be achieved by adjusting the duty cycle, the switching frequency, and/or the phase shift angle between the transformer primary and secondary voltages, as will be discussed in detail in the following sections. When power flows from the LVS to the HVS, the LVS converter is current-fed, or in other words, works in boost mode to keep the HVS voltage at a desired level. In the other direction of power flow, the HVS converter is voltage-fed, or works in buck mode, so that the battery absorbs the energy captured during the regenerative braking. The HVS switches are implemented with IGBTs, and the LVS switches are

MOSFETs because of their very low on-resistance at low voltage.

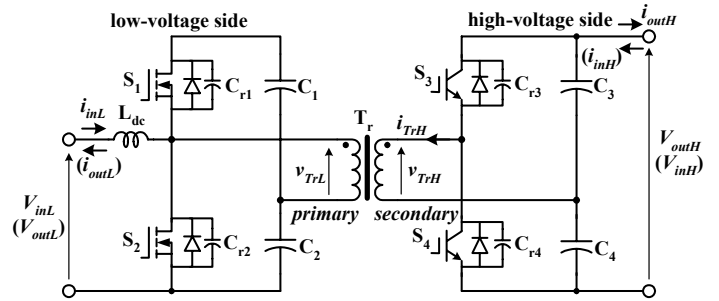


Fig. 2. Schematic of the soft-switched bi-directional dc/dc converter.

There is a snubber capacitor across each switch. The leakage inductance, together with the snubber capacitors, is also utilized to provide soft switching for the switches, eliminating the problems of interaction between the leakage inductance and diode reverse recovery. The resonance between the capacitors and the inductance enables the switches to turn on under zero current and voltage, while the snubber capacitors allow them to turn off at zero voltage.

In summary, this converter topology has the following features when compared to the dual–full-bridge counterpart:

- 1) The total device rating is the same as for the dual–full-bridge alternative at the same output power.
- 2) Although the devices of the LVS are subject to twice the dc input voltage, this is not a serious concern because the input voltage in the anticipated application is 12 V.
- 3) The dual–half-bridge topology uses only half as many devices as the full-bridge topology does.
- 4) No additional active switches are needed for soft-switching.

### B. Operating Principles

For soft-switching, the converter relies on a commutation mechanism similar to the diode-to-switch commutation of the auxiliary resonant commutated pole (ARCP) converter [10]; i.e., turn-off of the main conducting device diverts the current to the corresponding snubber capacitors to charge one and discharge the other, resulting in a zero voltage turn-off. The zero voltage turn-on is achieved by gating on the in-coming device while the anti-parallel diode is conducting. However, unlike the ARCP converter, the proposed converter does not require an auxiliary circuit to achieve soft switching. A step-by-step description of the soft-switching processes and soft-switching conditions are given in [9].

For the discussion of power flow control, a simplified, primary-referred equivalent circuit is drawn in Fig. 3, where the snubber capacitors are omitted for simplicity and  $L_s$  represents the leakage inductance of the transformer. Idealized voltage and current waveforms of the transformer are illustrated in Fig. 4. Power flows from the LVS to the HVS when

the phase of the transformer primary voltage  $v_{Tr1}$  supplied by the LVS half-bridge is leading the secondary voltage  $v_{Tr2}$  supplied by the HVS half-bridge. The converter thus works in the boost/discharge mode to power the HVS load. By making the phase of the secondary voltage  $v_{Tr2}$  leading the primary voltage  $v_{Tr1}$ , power flow can be reversed and the converter works in buck mode to recharge the LVS battery.

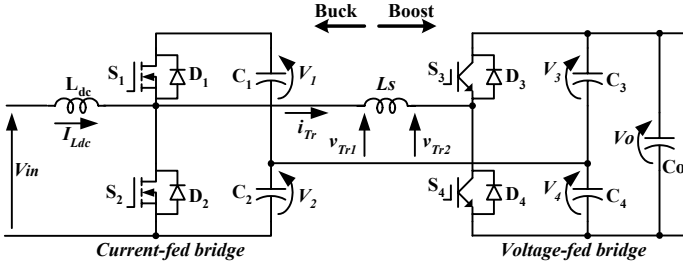


Fig. 3. A simplified, primary-referenced equivalent circuit.

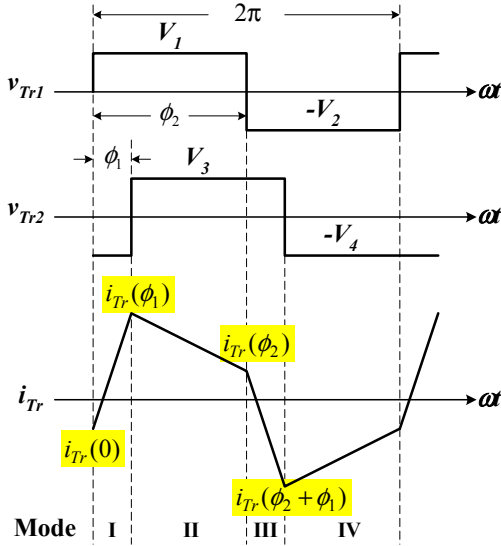


Fig. 4. Idealized voltage and current waveforms of transformer.

### III. DESIGN CONSIDERATIONS

#### A. Power Transfer Characteristics

The analysis of static characteristics is based on the primary-referenced equivalent circuit in Fig. 3 and the idealized waveforms in Fig. 4, where  $\phi_l$  represents the phase shift angle between the transformer primary and secondary voltages. There are four operation modes in one switching period, and the relationship between voltage and current in each mode can be established. Assuming the duty ratio is fixed at 50%, i.e.,  $\phi_2 = \pi$ , and  $V_1 = V_2 = V_{in}$ ,  $V_3 = V_4 = V_o/2$ , at steady state, the transferred power can be found to be:

$$P_o = \frac{V_{in} V_o \phi_l (\pi - \phi_l)}{2\omega L_s \pi} \quad (1)$$

Where  $\omega$  is the angular switching frequency,  $V_{in}$  the input dc voltage, and  $V_o$  the high-side dc bus voltage referred to the primary side.

Equation (1) indicates that, when duty cycle and switching frequency are fixed, the output power is related to phase shift angle and transformer leakage inductance. For a given amount of output power, a smaller leakage inductance results in a smaller phase shift angle. To reduce the circulating current and to improve the efficiency, the phase shift angle should be kept as small as possible. Therefore, the leakage inductance needs to be minimized. On the other hand, a higher leakage inductance helps to meet the soft-switching conditions.

#### B. Design Equations

For a given maximum output power,  $P_{o\_max}$ , at an input dc voltage,  $V_{in}$ , a switching frequency,  $\omega$ , an expected phase shift angle,  $\phi_l$ , the transformer leakage inductance,  $L_s$ , can be calculated by

$$L_s = \frac{V_{in} V_o \cdot \phi_l \cdot (\pi - \phi_l)}{P_{o\_max} \cdot 2\omega\pi} \quad (2)$$

Referring to Fig. 4, the initial states  $i_{Tr}(0)$ ,  $i_{Tr}(\phi_1)$ ,  $i_{Tr}(\phi_2)$ ,  $i_{Tr}(\phi_1 + \phi_2)$  for each of the four modes during one complete switching cycle can be derived based on the boundary conditions:

$$\begin{cases} i_{Tr}(0) = -i_{Tr}(\phi_2) \\ i_{Tr}(\phi_1) = -i_{Tr}(\phi_2 + \phi_1) \end{cases} \quad (3)$$

At a duty ratio of 50%, i.e.  $\phi_2 = \pi$ , the boundary points of  $i_{Tr}$  can be calculated by Eq. (4).

$$\begin{cases} i_{Tr}(0) = \frac{V_3 - V_1}{2\omega L_s} (\pi - \phi_1) - \frac{V_1 + V_4}{2\omega L_s} \phi_1 \\ i_{Tr}(\phi_1) = \frac{V_1 + V_4}{2\omega L_s} \phi_1 + \frac{V_3 - V_1}{2\omega L_s} (\pi - \phi_1) \\ i_{Tr}(\pi) = -i_{Tr}(0) \\ i_{Tr}(\pi + \phi_1) = -i_{Tr}(\phi_1) \end{cases} \quad (4)$$

Assuming an efficiency of  $\eta$ , the average current of  $I_{Ldc}$  provided by the battery can be found by

$$I_{Ldc} = \frac{P_{o\_max}}{\eta V_{in}} \quad (5)$$

While the LVS switches,  $S_1$  and  $S_2$ , share a voltage stress equal to the battery voltage,  $V_{in}$  at steady state, they bear unequal current stresses. The HVS switches share equal voltage and current stresses. The current ratings of the LVS devices can be determined based on the operating conditions and is

estimated by

$$\begin{cases} I_{S1(peak)} = I_{Ldc} - i_{Tr}(0) \\ I_{S2(peak)} = I_{Ldc} + i_{Tr}(\phi_1) \end{cases} \quad (6)$$

The maximum and minimum voltage change rates,  $dv/dt$ , happen at  $\omega t=0$ , where the turn-off current is maximum, and  $\omega t=\pi$ , where the turn-off current becomes minimum, respectively. Assuming the snubber capacitance is  $C_r$ , the range of  $dv/dt$  can be derived as

$$\frac{|i_{Tr}(\pi)| - |I_{Ldc}|}{C_r} \leq \frac{dv}{dt} \leq \frac{|i_{Tr}(0)| + |I_{Ldc}|}{C_r} \quad (7)$$

The inductance  $L_{dc}$  can be determined for a given peak-to-peak ripple current,  $\Delta I$  of  $I_{Ldc}$  by

$$L_{dc} = \frac{V_{in}}{2 f_{sw} \cdot \Delta I} \quad (8)$$

While aforementioned equations are for a fixed duty ratio of 50 %, the duty ratio can also be adjusted to control the amount of power to be transferred. Detailed discussion will be given in future publications.

#### IV. EXPERIMENTAL RESULTS

A 1.6 kW prototype has been built and tested to evaluate its performance. Fig. 5 shows a photo of the prototype. In order to compare with the size of the first-generation converter, the prototype is laid on a 0.375" liquid-cooled heat sink with the same footprint, 7.5" in width by 13.5" in length. The actual occupied area is 7.25" by 8.5", illustrating the high power

density characteristic of the second-generation converter. A switching frequency of 20 kHz is chosen for the MOSFETs and IGBTs to make the best use of the IGBT switches. The leakage inductance of the transformer in this prototype was measured as 0.4  $\mu$ H. Power flow control is implemented with a digital signal processor.

Typical oscillograms in boost mode, i.e. charging the high voltage side from the low voltage, are given in Fig. 6. Fig. 6(a) shows, from the top toward the bottom, the low side input voltage,  $V_{inL}$ , input current,  $I_{inL}$ , high side output voltage,  $V_{outH}$ , output current,  $I_{outH}$  and (b) shows  $V_{inL}$ , the transformer primary side voltage,  $V_{TrL}$ , secondary voltage,  $V_{TrH}$  and current,  $i_{TrH}$ . Fig. 6(c) and (d) are time expanded oscillograms showing  $V_{inL}$ , and the transformer primary and secondary voltages,  $v_{TrL}$  and  $v_{TrH}$ , and current,  $i_{TrH}$  during switching transitions. The slowly changing slopes of the transformer voltages indicate that soft-switching is achieved.

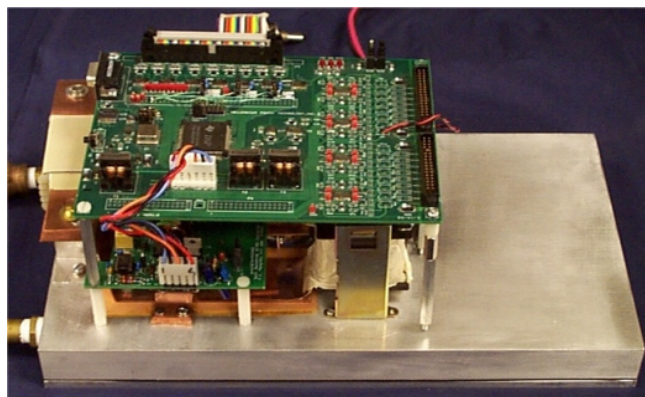
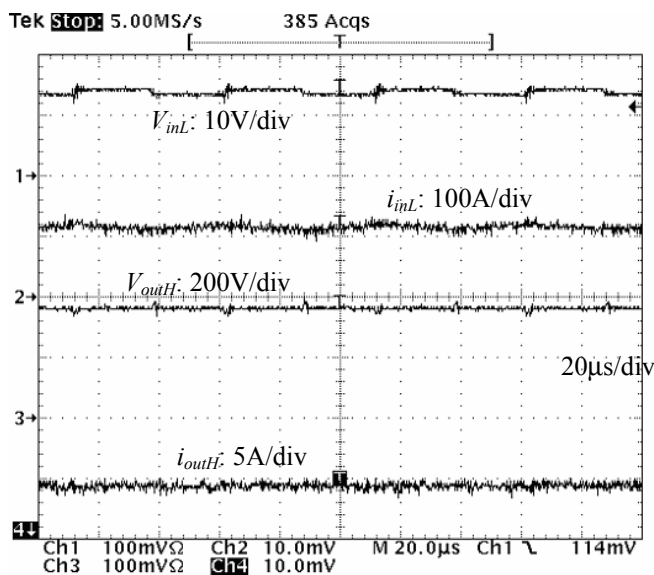
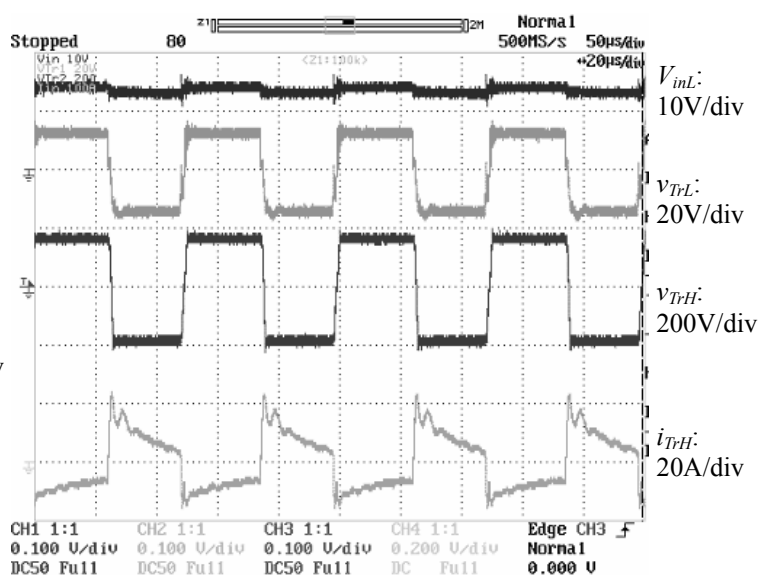


Fig. 5. Photo of the prototype.



(a) Input, output current and voltage waveforms



(b) Transformer current and voltage waveforms

Fig. 6. Steady state waveforms in low-to-high conversion mode; load power: 1.42 kW, efficiency: 92%.

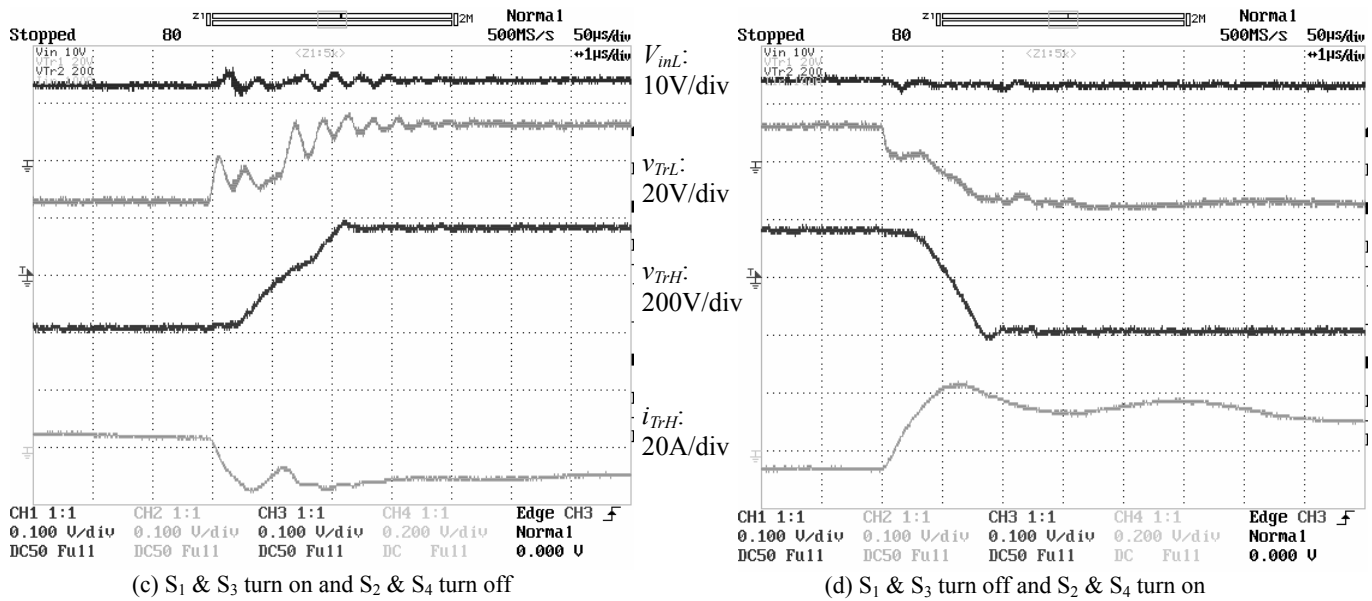


Fig. 6 Steady state waveforms in low-to-high conversion mode; load power: 1.42 kW, efficiency: 92%.

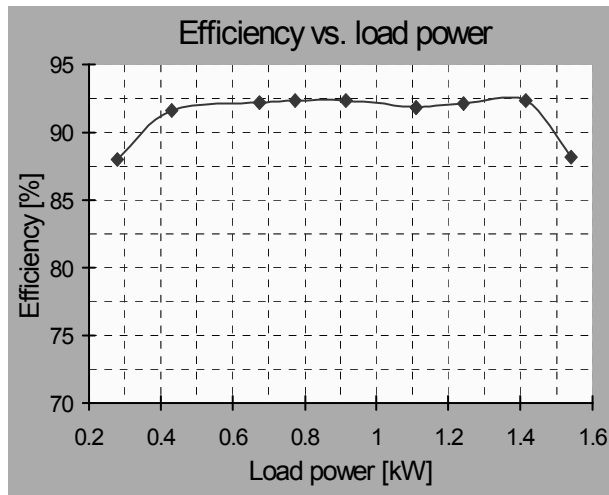


Fig. 7. Efficiency chart for low-to-high conversion.

Fig.7 plots an efficiency chart in the boost mode. Efficiency is above 92% over a range of output power form 0.45 kW to 1.4 kW.

Duty ratio control was employed in the buck mode, i.e. charging the low voltage side from the high voltage. Typical testing waveforms are given in Fig. 8, where 1.2 kW of power was transferred to a resistive load at the LVS. Fig. 8(a) shows, from the top toward the bottom, the high side input voltage,  $V_{inH}$ , input current,  $I_{inH}$ , low side output voltage,  $V_{outL}$ , output current,  $I_{outL}$ , and (b) shows the voltage across the witch  $S_2$ ,  $V_{S2}$ , the transformer primary side voltage,  $V_{TrL}$ , secondary voltage,  $V_{TrH}$  and current,  $i_{TrH}$ . Fig. 8(c) and (d) are time expanded oscillograms showing  $S_2$  voltage,  $V_{S2}$ , and the transformer primary and secondary voltages,  $v_{TrL}$  and  $v_{TrH}$ , and current,  $i_{TrH}$  during switching

transitions. The slowly changing slopes of the transformer voltages indicate that soft-switching is achieved.

## V. CONCLUSIONS

The soft-switched bi-directional dc/dc converter developed for FCPEV applications has the following features:

- A small number of switching devices. Compared with the full-bridge topologies, this converter has half the number of switching devices. This reduction also leads to significant savings on the gate drive and accessory power requirements.
- No auxiliary circuit or complex control dedicated for soft switching.

A prototype rated at 1.6 kW was designed, built, and successfully tested in the laboratory. This topology, therefore, provides a solution for low-cost, lightweight, compact, and reliable dc/dc converter designs for automotive applications. Other application areas are in uninterrupted power supplies and battery charging and discharging systems.

## REFERENCES

- [1] T. Gilchrist, "Fuel cells to the fore," *IEEE Spectrum*, November 1998.
- [2] R. L. Steigerwald, "High-frequency resonant transistor dc/dc converters," *IEEE Trans. Ind. Electron.*, Vol. IE-3, no. 2, pp.181–191, May 1984.
- [3] M. Jain, M. Daniele and P. K. Jain, "A bidirectional dc-dc converter topology for low power application," *IEEE Trans. Power Electronics*, vol.15, No.4, pp. 595–606, July 2000.
- [4] T. Reimann, S. Szeponik, G. Berger, and J. Petzoldt, "A novel

control principle of bi-directional dc/dc power conversion,” in Conf. Rec. 1997 IEEE Power Electronics Specialist Conf., pp. 978–984.

- [5] M. Divan and O. Patterson, “A pseudo resonant full bridge dc/dc converter,” in Conf. Rec. 1987 IEEE Power Electronics Specialist Conf., pp.424–430.
- [6] R. Watson et al., “A soft-switched, full-bridge boost converter employing an active-clamp circuit,” in Conf. Rec. 1996 IEEE Power Electronics Specialist Conf., pp.1948–1954.
- [7] R. W. DeDonker, D. M. Divan, and Kheraluwala, “Power conversion apparatus for dc/dc conversion using dual active

bridges,” U. S. Patent, no. 5,027,264

- [8] M. H. K. Wang et al, “Bi-directional dc to dc converters for fuel cell systems,” in Conf. Rec. 1998 IEEE Power Electronics In Transportation, pp. 47–51.
- [9] H. Li, Fang Z. Peng, and J. Lawler, “Modeling, simulation, and experimental verification of soft-switched bi-directional DC-DC converters,” IEEE APEC proceeding, 2001, pp.736–742.
- [10] R. W. DeDonker and J. P. Lyons, “The auxiliary resonant commutated pole converter,” *IEEE IAS Annu. Meet. Conf. Rec.*, pp. 1228–1235, 1990.

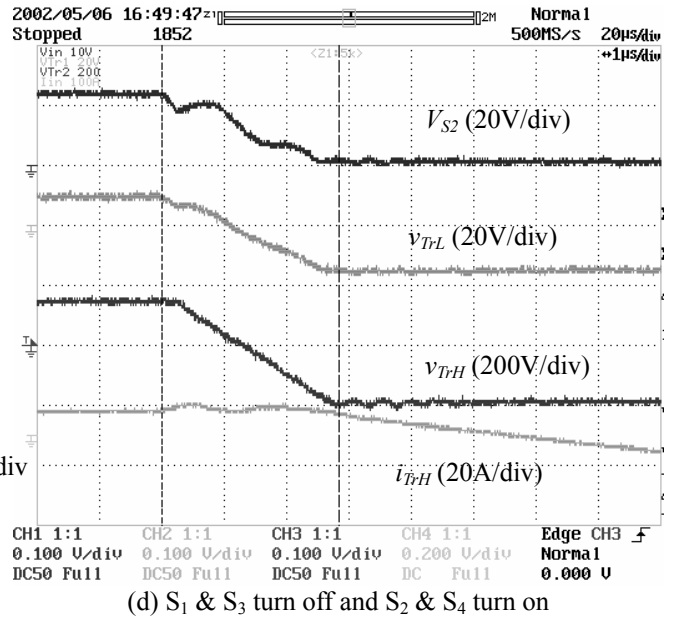
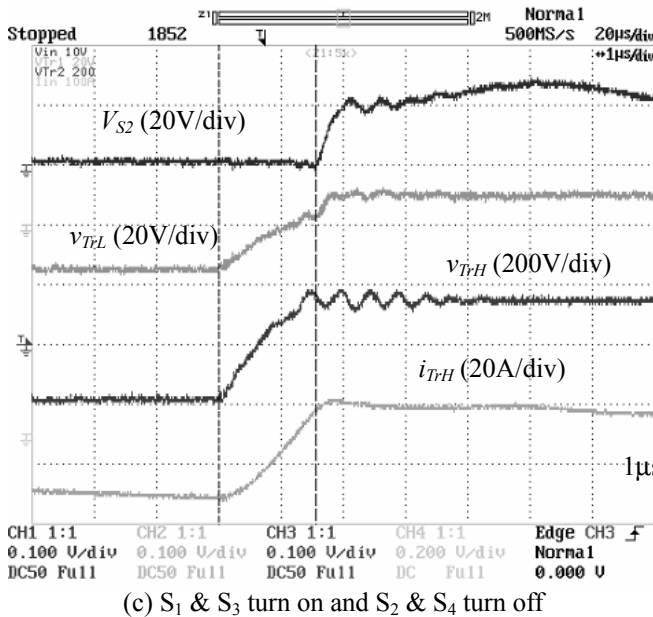
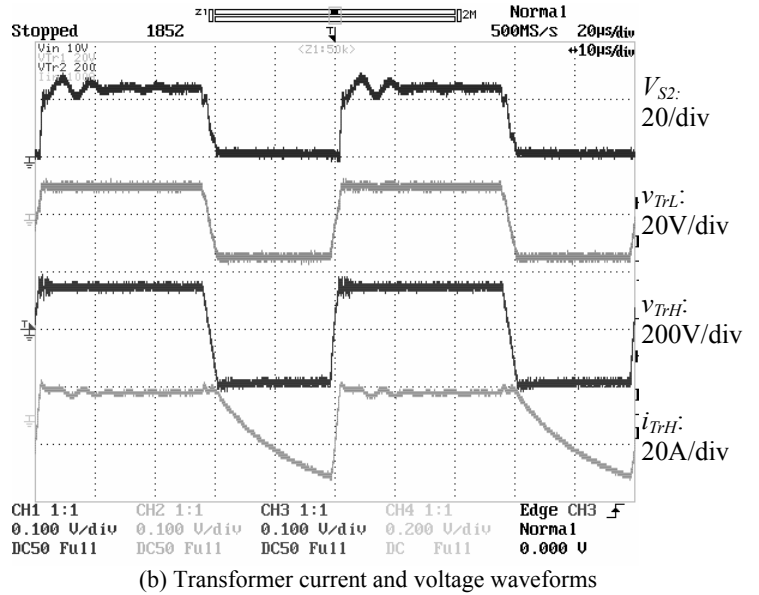
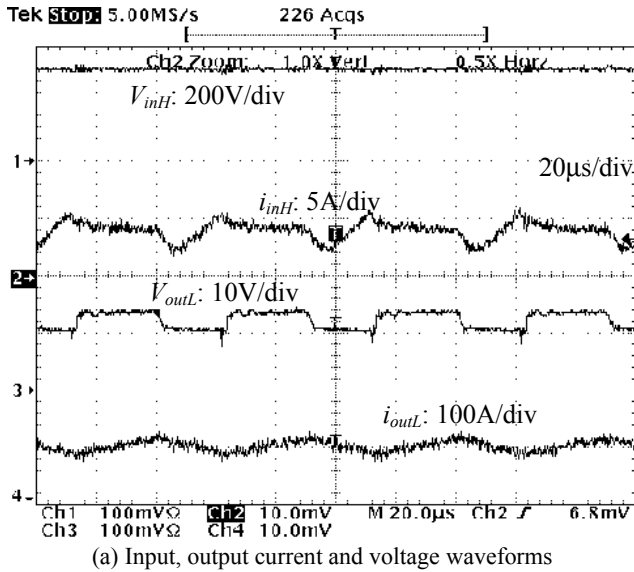


Fig. 8. Time expanded oscillograms showing soft-switching in high-to-low conversion.